# Lidar Measurement of Wind Velocity Profiles in the Boundary Layer

JEFFERY T. SROGA AND EDWIN W. ELORANTA

*Department of Meteorology, University of Wisconsin, Madison 53706*

TED BARBER

*Atmospheric Sciences Laboratory, White Sands Missile Range, NM 88002*

(Manuscript received 5 September 1979, in final form 31 January 1980)

ABSTRACT

A lidar technique for measuring wind in the atmospheric boundary is presented. Inhomogeneities in ambient aerosol content are used as tracers of the wind. This technique yields both horizontal components of the wind and the wind velocity variance. These results are achieved using a model which assumes an isotropic Gaussian distribution of turbulent velocities. Experimental results comparing lidar wind measurements with winds derived from radar-tracked pilot balloons and tower-mounted anemometers show good agreement. Wind measurements have been obtained at slant range distances up to 6.5 km.

## 1. Introduction

Knowledge of the wind structure in the earth's planetary boundary layer is essential for many meteorological applications. Aviation, air pollution and boundary-layer meteorology require spatial and temporal resolution in wind velocity measurements. Remote sounding techniques offer the possibility of measuring wind velocities in large volumes of the atmosphere on a continuous basis. These measurements are not influenced by the physical presence of the sensor.

Lidar signals backscattered from the planetary boundary layer are dominated by scattering from aerosol particles. The aerosol content of the lower atmosphere fluctuates under the continuous influence of particle sources and particle deposition mechanisms. These fluctuations in aerosol content are easily detected with lidar. By observing the drift of these spatial inhomogeneities, lidar can be used to determine wind velocities remotely. Correlation techniques using lidar profiles of aerosol backscatter intensity have been used to remotely measure winds by Derr and Little (1970), Eloranta *et al.* (1975) and Armstrong *et al.* (1976).

The wind measurement technique described in this study uses the lidar geometry shown in Fig. 1. The lidar is elevated by a small angle and is rapidly scanned between three closely spaced azimuth angles. Lidar data consist of a time series of lidar profiles obtained at each of the three azimuth angles. The horizontal wind component perpendicular to the lidar beam is obtained by measuring the time interval needed for aerosol inhomogeneities to drift from one azimuth angle to the next. The longitudinal component of the wind is determined from the radial displacement which occurs during this cross-path drift time. The cross-path drift time and radial displacement are measured using a fast Fourier transform technique. This method is equivalent to measuring the space-time correlation function of lidar profiles to infer winds as was done by Eloranta *et al.* (1975) and Kunkel *et al.* (1980).

Because of spatial and temporal fluctuations in velocity, the maximum value of the aerosol correlation function between profiles obtained at different azimuth angles decreases with increasing angular separation. A simple model describing this effect is used to measure the magnitude of the turbulent velocity fluctuations.

Lidar wind measurements are derived from the drift of aerosol inhomogeneities with spatial dimensions ranging between ~15 and 500 m. Typical measurements involve spatial averaging over range intervals of 250 to 1000 m and time averages of 2 to 5 min.

## 2. Procedure

Profiles of aerosol backscattering are obtained with the University of Wisconsin lidar system (see Table 1). The return power measured with this system is given by

$$P(\phi,R,t_n) = E_n \frac{c}{2}\frac{A_r}{R^2}\beta_s(\phi,R,t_n)\frac{P'(\phi,R,t_n)}{4\pi} \times \exp\left[-2\int_0^R \beta_e(\phi,R',t_n)dR'\right], \quad (1)$$

where

0021-8952/80/050598-08$06.00

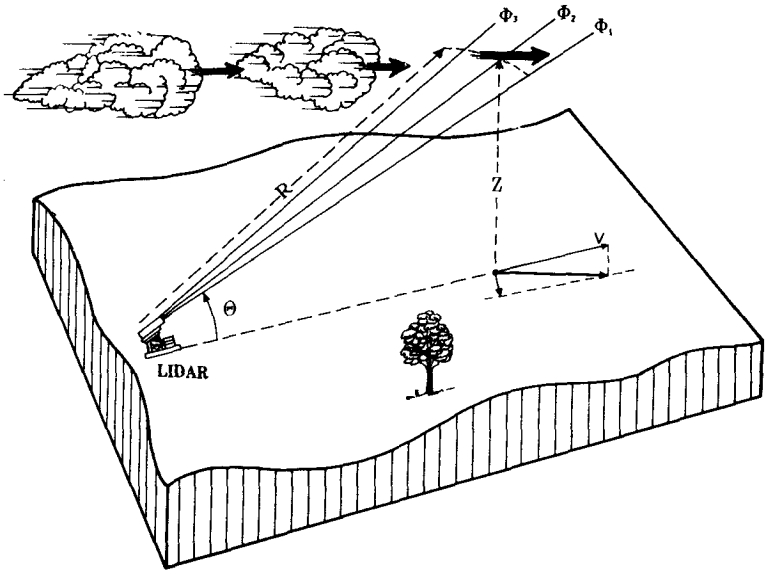


FIG. 1. The geometry used for lidar wind measurements. The lidar is operated at a constant small elevation angle and scanned back and forth between three closely spaced azimuth angles $\phi_1$, $\phi_2$ and $\phi_3$. Range-resolved profiles of backscattered intensity are recorded at ~1 s intervals for a period of 2–5 min to produce a wind measurement. Wind velocities are calculated in terms of a radial component $v$ and a cross-path component $u$.

| | |
|---|---|
| $P(\phi,R,t_n)$ | instantaneous received power from range $R$ |
| $R$ | radial distance along propagation path |
| $\phi$ | azimuth angle of lidar profile |
| $t_n$ | time of $n$th lidar profile |
| $E_n$ | transmitted energy of the $n$th laser pulse |
| $A_r$ | area of the receiver telescope |
| $c$ | speed of light |
| $\beta_s(\phi,R,t_n)$ | scattering cross section per unit volume |
| $\beta_\epsilon(\phi,R,t_n)$ | extinction cross section per unit volume |
| $P'(\phi,R,t_n)$ | aerosol phase function for backscattering |

This lidar return signal is logarithmically amplified to compress the dynamic range and digitized into 10-bit words at a 10 MHz rate, yielding a 15 m range resolution.

The sequential three-angle azimuth scan shown in Fig. 1 ($\phi = \phi_1, \phi_2, \phi_3, \phi_2, \phi_1, \phi_2, \ldots$) yields three separate time series of lidar profiles, $P(\phi,R_l,t_n)$. These profiles are corrected for the inverse range squared dependence of the lidar equation and normalized by the transmitted laser pulse energy. At each azimuth angle a time-centered running mean profile is subtracted from the normalized return; this procedure yields the aerosol inhomogeneity profiles $Y(\phi,R_l,t_n)$:

$$Y(\phi,R_l,t_n) = \left[\frac{R_l^2 P(\phi,R_l,t_n)}{E_n}\right] - \frac{1}{2m+1}\sum_{i=-m}^{m}\left[\frac{R_l^2 P(\phi,R_l,t_{n+i})}{E_{n+i}}\right], \quad (2)$$

where $R_l$ is the range to the $l$th data point and $2m + 1$ the number of lidar profiles at each azimuth $\phi$ used in calculating the mean aerosol structure. The range-averaged mean value within each data segment is removed as follows:

$$Y'(\phi,R_l,t_n) = Y(\phi,R_l,t_n) - N^{-1}\sum_{i=a}^{b} Y(\phi,R_i,t_n), \quad (3)$$

where the data segment extends from data point $l = a$ to $l = b$ and where $N = b - a$.

TABLE 1. University of Wisconsin lidar system parameters (1978).

| | |
|---|---|
| *Transmitter* | |
| Wavelength | 694.3 nm (ruby) |
| Output energy | 1.0–1.5 J per pulse |
| Pulse duration | 20 ns (Pockels cell $Q$-switched) |
| Beam divergence | 1 mrad |
| Repetition rate | 1 Hz (max) |
| *Receiver* | |
| Telescope | 31 m Newtonian |
| Field of view | Adjustable (1.5–7 mrad) |
| Detector | RCA C70042K PMT |
| Quantum efficiency | 6.8% @ 694.3 nm |
| Spectral bandpass | 1.0 nm (interference filter) |
| *Data logging* | |
| Logarithmic amplifier | 60 μV to 0.6 V input range |
| A/D conversion | 10 bit resolution |
| Sampling rate | 10 MHz |
| Range resolution | 15 m |
| Preprocessing | PDP 11/40 minicomputer |
| Output | Magnetic tape, real-time display |

These aerosol inhomogeneity profiles are then transformed into spatial wave number space using the fast Fourier transform. A cosine taper on 10% of each end of the aerosol inhomogeneity data segment is applied to reduce leakage in the spectral estimates (Bingham *et al.*, 1967). The Fourier transform of the aerosol inhomogeneity profile from the spatial coordinate $R_l$ to the wavenumber coordinate $k$ is

$$F(\phi,k,t_n) = \sum_{l=a}^{b} Y'(\phi,R_l,t_n) \exp(-2\pi ikR_l). \quad (4)$$

These transformed profiles are then used to compute raw cross-spectral estimates between profiles for all combinations of angles $(\phi_i,\phi_j)$ and for all time separations $(\Delta t)$ corresponding to possible cross-path drift times:

$$S(\phi_i,\phi_j,k,t_n,\Delta t) = F^*(\phi_i,k,t_n)F(\phi_j, k, t_n + \Delta t), \quad (5)$$

where an asterisk denotes the complex conjugate and $S(\phi_i,\phi_j,k,t_n,\Delta t)$ is the raw cross-spectral estimate. Smooth spectral estimates are obtained by time-averaging the raw spatial spectral estimates to increase the statistical significance (Welsh, 1967). The cross-spectral estimate averaged over $J$ profiles is given by

$$\tilde{S}(\phi_i,\phi_j,k,\Delta t) = J^{-1} \sum_{n=1}^{J} S(\phi_i,\phi_j,k,t_n,\Delta t). \quad (6)$$

The coherence which measures the degree of correlation as a function of the spatial wavenumber $k$ is used to determine the time for the aerosol inhomogeneities to drift between the different azimuthal angles. The coherence calculated from the smoothed spectral estimates (Otness and Enochson, 1972) is

$$\mathrm{coh}(k,\Delta x,\Delta t) = \frac{\tilde{S}^*(\phi_i,\phi_j,k,\Delta t)\tilde{S}(\phi_i,\phi_j,k,\Delta t)}{\tilde{S}(\phi_i,\phi_i,k,0)\tilde{S}(\phi_j,\phi_j,k,0)}. \quad (7)$$

The average lateral separation $\Delta x$ and mean height $\bar{Z}$ of a data segment are given by

$$\left.\begin{aligned} \Delta x &= 2\bar{R} \sin[(\phi_i - \phi_j)/2] \\ \bar{Z} &= \bar{R} \sin\theta \end{aligned}\right\}, \quad (8)$$

where $\bar{R}$ is the mean radial distance of the data segment and $\theta$ the elevation angle of the lidar (Fig. 1).

Because of noise in lidar measurements, each spectral component does not contain the same information on wind motion. Spatial filtering of lidar profiles is required to enhance the signal characteristics of the aerosol density inhomogeneities over the background noise level. A filter which suppresses noise while minimizing the error in reproducing this signal can be calculated from knowledge of the spectral characteristics of the signal and noise contributions (Wainstein and Zubakov, 1962). When the signal and noise are uncorrelated, the Fourier transform $H(k)$ of the optimal linear filter is

$$H(k) = \frac{\tilde{S}_S(k)}{\tilde{S}_S(k) + \tilde{S}_N(k)}, \quad (9)$$

where $\tilde{S}_S(k)$ and $\tilde{S}_N(k)$ are the signal and noise power spectra. This optimal transfer function can be estimated from the lidar data. Lidar power spectral estimates are the sum of the aerosol inhomogeneity spectrum and noise spectrum, i.e.,

$$\tilde{S}(\phi_i,\phi_i,k,0) = \tilde{S}_S(\phi_i,\phi_i,k,0) + \tilde{S}_N(\phi_i,\phi_i,k,0). \quad (10)$$

Because the noise in one profile is not correlated with the noise in other profiles, smooth cross-spectral estimates of lidar measurements suppress noise contributions. For the cross-spectral estimates with $\phi_i = \phi_j$, (i.e., $\Delta x = 0$) the limiting value as $\Delta t$ approaches zero is the signal power spectrum

$$\lim_{\Delta t \to 0} \tilde{S}(\phi_i,\phi_i,k,\Delta t) = \tilde{S}_S(\phi_i,\phi_i,k,0). \quad (11)$$

Using Eqs. (7), (9) and (11), the transfer function of the optimal linear filter is

$$H(k) = [\lim_{\Delta t \to 0} \mathrm{coh}(k,0,\Delta t)]^{1/2}. \quad (12)$$

The extrapolation of coherence measurements to $\Delta t = 0$ is performed with a least-squares regression to a Gaussian for each spectral component.

The transfer function $H(k)$ provides a method for calculating a weighted average of the coherence, $\overline{\mathrm{coh}}(\Delta x,\Delta t)$, which optimizes the overall signal-to-noise ratio:

$$\overline{\mathrm{coh}}(\Delta x,\Delta t) = \sum_{k=k_1}^{k_m} W(k) \mathrm{coh}(k,\Delta x,\Delta t), \quad (13)$$

where $W(k)$ is the normalized weighting function

$$W(k) = H^2(k)[\sum_{k=k_1}^{k_m} H^2(k)]^{-1} \quad (14)$$

and $k_1$ and $k_m$ are given by the fundamental wavelength $[k_1 = (N \times 15\ \mathrm{m})^{-1}]$ and the Nyquist spatial frequency $[k_m = (15\ \mathrm{m})^{-1}]$.

The signal-to-noise ratio [SNR$(k)$] can be estimated for each wavenumber by solving Eqs. (9) and (12) for $\tilde{S}_S(k)/\tilde{S}_N(k)$:

$$\mathrm{SNR}(k) = \tilde{S}_S(k)/\tilde{S}_N(k) = [\mathrm{coh}^{-1/2}(k,0,0) - 1]^{-1}. \quad (15)$$

Fig. 2 shows the signal-to-noise ratio and the square of the optimal filter as a function of wavenumber for data obtained on 19 January 1978 at White Sands Missile Range, New Mexico. In this case, the signal-to-noise ratio decreases by approximately two orders of magnitude as aerosol inhomogeneities vary from a scale size of 1 km to 30 m. Clearly, the weighting function $W(k)$ provides a substantial improvement in overall signal to noise ratio.

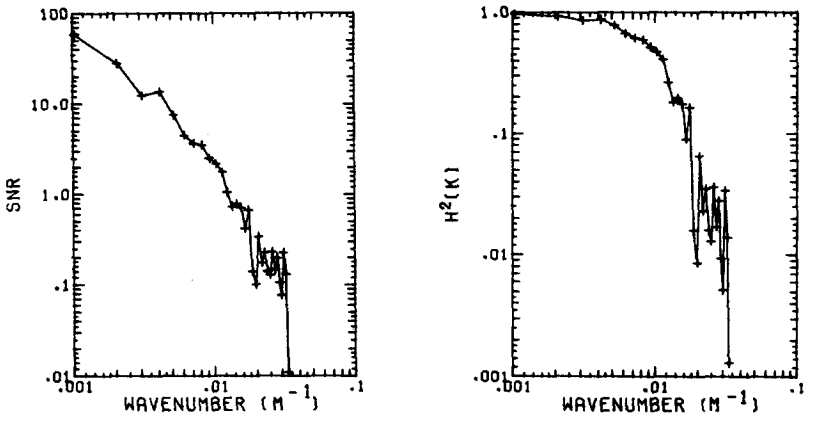


FIG. 2. The signal-to-noise ratio as a function of wavenumber and the optimal filter estimated from Eqs. (15) and (12), respectively, for data obtained on 19 January 1978 at White Sands, New Mexico.

A wavenumber averaged signal-to-noise ratio ($\overline{\text{SNR}}$) can be used to provide an objective criteria for rejecting wind determinations derived from noise dominated data, i.e.,

$$\overline{\text{SNR}} = \sum_{k=k_1}^{k_m} W(k)\,\text{SNR}(k). \tag{16}$$

If the wind were constant in space and time, the mean cross-path velocity $\bar{u}$ could be determined from $\bar{u} = \Delta x/\Delta t_{\max}$, where $\Delta t_{\max}$ is the time lag at which the weighted coherence [Eq. (13)] is largest. In practice, wind velocity fluctuations cause the coherence maximum to decrease with increases in either $\Delta x$ or $\Delta t$. As a result, the coherence maximum occurs at a time delay shorter than the cross-path drift time. A model similar to the one employed by Kunkel *et al.* (1980) is used to correct for this effect. It assumes that the spatial distribution of the aerosol density is Guassian and isotropic, and that these three-dimensional inhomogeneities are advected by a mean velocity plus a turbulent velocity with an isotropic Gaussian probability distribution. The functional form of this model is (Sroga, 1979)

$$\overline{\text{coh}}(\Delta x,\Delta t) = A\left[\frac{2\sigma_a^2}{2\sigma_a^2 + \sigma_s^2\Delta t^2}\right] \times \exp[-(\Delta x - \bar{u}\Delta t)^2/(2\sigma_a^2 + \sigma_s^2\Delta t^2)] \times \sum_{k=k_1}^{k_m} W(k)\exp(-4\pi^2k^2\sigma_s^2\Delta t^2), \tag{17}$$

where

$\overline{\text{coh}}(\Delta x,\Delta t)$ weighted coherence averaged over wavenumber
$A$ amplitude factor ($A \leq 1$)
$\bar{u}$ mean lateral wind speed
$\sigma_a$ rms horizontal width of the aerosol inhomogeneities
$\sigma_s$ rms width of the isotropic Gaussian velocity distribution [$\sigma_s^2 = u'^2 = v'^2 = w'^2$].

A nonlinear regression of Eq. (17) to measured weighted coherence values is used to estimate $A$, $\bar{u}$, $\sigma_a$ and $\sigma_s$. Initial values of these parameters must be estimated for the regression algorithm.

$A$, $\sigma_a$ and $\sigma_s$ are estimated as follows:

$A$ weighted coherence at $\Delta x = 0$, $\Delta t = 0$
$\sigma_a$ least-squares fit to Eq. (17) for data points near $\Delta t = 0$ and for $\Delta x = 0$
$\sigma_s$ 25% of the estimated mean wind speed.

A first approximation to the lateral velocity component $\bar{u}$ can be obtained from the time delay $\Delta t_e$ when the weighted coherence at zero separation is equal to the weighted coherence at separation $\Delta x$, i.e.,

$$\bar{u} = \Delta x/2\Delta t_e, \tag{18}$$

where $\Delta t_e$ is obtained as shown in Fig. 3. Eq. (18) is derived, following Briggs *et al.* (1950) from Eq. (17) by setting

$$\overline{\text{coh}}(0,\Delta t_e) = \overline{\text{coh}}(\Delta x,\Delta t_e). \tag{19}$$

Data points for the regression analysis are chosen about the maximum weighted coherence for each lateral separation. An example of the measured weighted coherence and the fit provided by this regression is presented in Fig. 3. The inability of this model to fit the data exactly is due to limitations in the Gaussian approximations employed in the derivation of Eq. (17). This model is used, despite its shortcomings, because it is easily applied and has been shown to provide reasonable values for $\bar{u}$ and $\sigma_s$. [A more complete discussion of this modeling problem in the case of grid generated turbulence can be found in Comte-Bellot *et al.* (1971).]

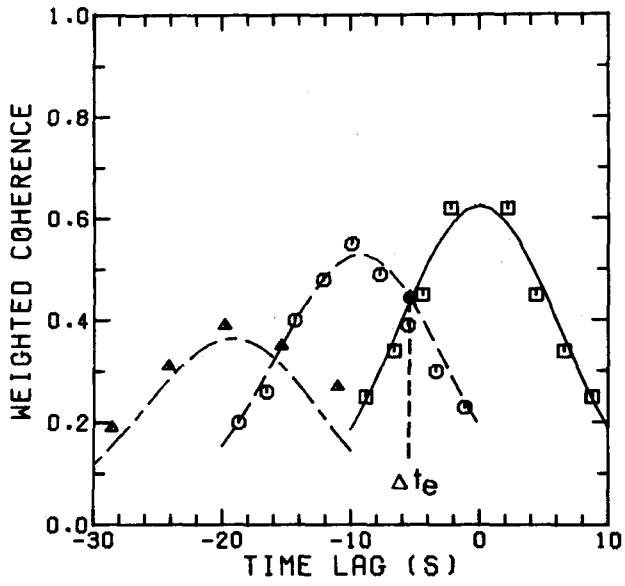


FIG. 3. An example of the weighted coherence [Eq. (13)] as a function of time lag for three lateral separations, $\Delta x$ = 0 m (□), $\Delta x$ = 38 m (○), $\Delta x$ = 76 m (△). A least-squares regression of Eq. (17) to the data is shown by lines on the graph. The time lag $\Delta t_e$ when the weighted coherence for zero angular separation and the 1° angular separation are equal is used with Eq. (18) to provide a first estimate of the cross path wind.

The horizontal projection of the average radial velocity is obtained from the phase of the smoothed cross spectra:

$$\bar{v} = m^{-1} \sum_{k=k_1}^{k_m} W(k) v_r(k) \cos\theta, \qquad (20)$$

where $v_r(k) = \Delta\psi(k)/(2\pi k \Delta t)$ radial velocity of wavenumber $k$ and $\Delta\psi(k)$ is the phase (rad) of the smoothed cross spectrum. The mean wind speed and direction are calculated from

$$V_{\text{lidar}} = (\bar{u}^2 + \bar{v}^2)^{1/2}, \qquad (21)$$

$$\phi_{\text{lidar}} = 180° + \phi_2 + \tan^{-1}(\bar{u}/\bar{v}), \qquad (22)$$

where $\phi_2$ is shown in Fig. 1.

### 3. Experimental results

Remote wind measurement experiments were conducted in Madison, Wisconsin and at the White Sands Missile Range, New Mexico. All lidar measurements were obtained using a three angle azimuthal scan with a 1.0° azimuth separation and a laser repetition rate of 0.9 Hz. Each lidar wind determination was calculated from aerosol inhomogeneity cross spectra smoothed over a 5 min time interval.

Lidar measurements obtained in Madison were compared to a bivane anemometer (R. M. Young model 21002) mounted on a radio tower located 2.7 km from the lidar. The lidar beam pattern was centered on the tower, with the lidar operated at a 2.3° elevation angle in order to place the lidar beam at the same altitude (77 m) as the anemometer. The anemometer signals were digitized and recorded at a 1 Hz rate; wind speed and direction were obtained by averaging radial and cross-beam components of the wind over the 5 min periods of the lidar measurements. Anemometer measurements of $\sigma_s$ were calculated from the rms mean of the turbulent velocity components $u$, $v$ and $w$, i.e.,

$$\sigma_{s(\text{tower})} = [(\overline{u'^2} + \overline{v'^2} + \overline{w'^2})/3]^{1/2}. \qquad (23)$$

All Madison wind comparisons were made on clear sunny days. Fig. 4 shows a time history of lidar- and tower-measured winds obtained on 20 June 1977. Fig. 5 presents a comparison of lidar and anemometer measurements of wind speed, direction and rms fluctuations $\sigma_s$ for six separate days. All lidar measurements made on these days with $\overline{\text{SNR}} > 0.5$ are presented.

Although it is rather difficult to estimate reliable confidence limits for lidar measurements, error bars have been plotted in Fig. 5. The lidar error estimates show the combined effects of a ±1.1 s error (one laser shot interval) in measuring the cross-path drift time and a ±15 m (one data point) error in determining the phase shift of the cross spectra. The error bars for the lidar $\sigma_s$ measurements are 95% confidence limits provided by the nonlinear regression procedure.

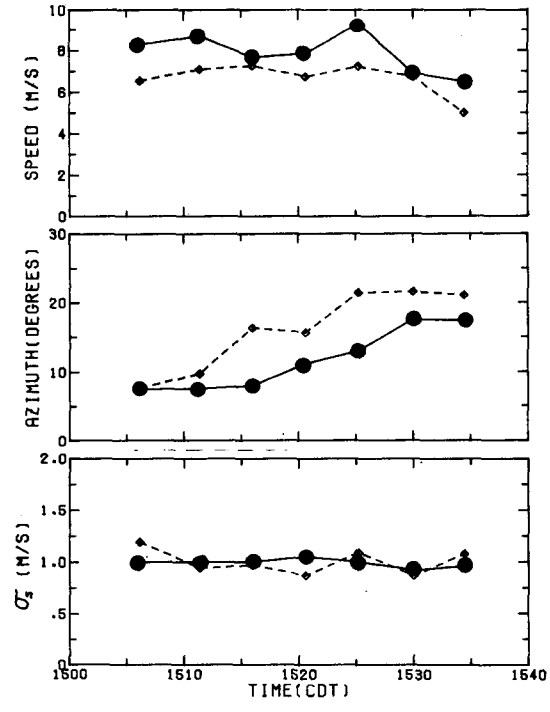


FIG. 4. A time history comparison of winds measured on 20 June 1977 with lidar (solid lines) and a tower-mounted anemometer (dashed line). These measurements were obtained on a clear day at Madison, Wisconsin.

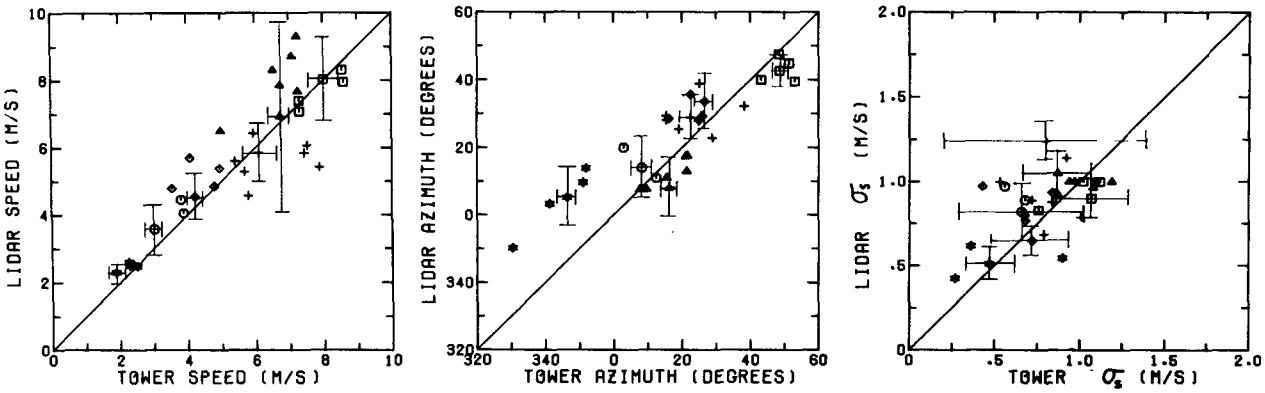


FIG. 5. A comparison of winds measured under clear convective conditions at Madison, Wisconsin with lidar and a tower mounted anemometer on 22 April (□), 23 May (○), 20 June (△), 23 June (+), 27 June (◇) and 27 July (☆), 1977. The anemometer was centered within the lidar measurement volume and all measurements were averaged over the same time interval. Estimates of the uncertainty in both lidar and anemometer measurements are shown for each day.

We believe that largest error source in the anemometer measurement is not due to intrinsic instrumental error but rather the uncertainty of comparing a measurement made at a single point with the 1 km spatial average obtained with the lidar. The error bars for the anemometer derived winds show the expected errors $(\Delta u, \Delta v)$ in determining the ensemble average wind from a 5 min single point average:

$$\Delta u = \left(\overline{u'^2}\,\frac{5\text{ min}}{\tau_E}\right)^{1/2}, \tag{24}$$

$$\Delta v = \left(\overline{v'^2}\,\frac{5\text{ min}}{\tau_E}\right)^{1/2}, \tag{25}$$

where $\overline{u'^2}$, $\overline{v'^2}$ and the Eulerian time scale $\tau_E$ (Csanady, 1973), are measured from tower data segments of ~30 min duration. The error bars for the tower measurements of $\sigma_s$ are given by the fluctuations of sigma values measured in five or six 5 min segments near the time of the tower measurement.

Lidar measurements made in Madison are consistent with concurrent tower measurements. The rms differences in speed and azimuth were 1.0 m $s^{-1}$ and 10° respectively. These errors are roughly consistent with the errors expected due to discrete temporal and spatial sampling of the lidar along with errors in estimating a volume averaged wind with a single point sampling.

At White Sands wind velocity profiles derived from radar-tracked pilot balloons were used to verify lidar wind measurements. Measurements on 19 January 1978 occurred under conditions of very light snow. These data are characterized by large fluctuations in the observed lidar profiles. They provide a test of lidar wind measurement algorithms without the need to separate small signals from noise. Wind measurements within vertical intervals of ~100 m were obtained by operating the lidar at a 6° elevation angle and dividing the lidar profiles into 960 m range intervals. For comparison the pilot balloon measurements were averaged over the same height intervals as the lidar. Fig. 6 shows one

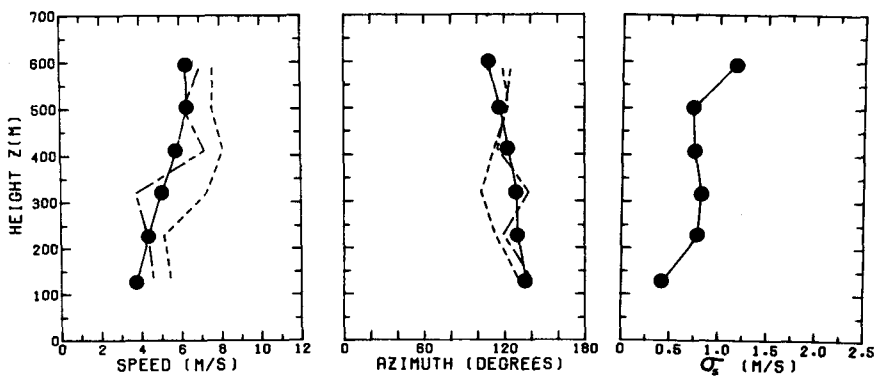


FIG. 6. A comparison of lidar and pilot balloon wind measurements at White Sands, New Mexico on 19 January 1978. Lidar data were obtained between 1652 and 1657 MST and is plotted with solid lines. Pilot balloons are at 1645–1647 MST (– – –) and 1655–1657 (— — —).

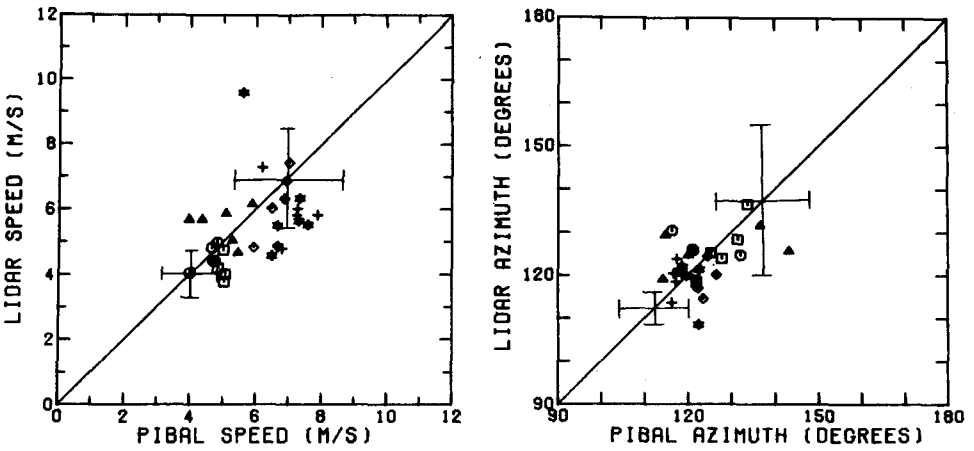


FIG. 7. A comparison of winds measured at White Sands, New Mexico with lidar and radar-tracked pilot balloons. All measurements were made during a light snowfall on 19 January 1978. Lidar and balloon measurements represent vertical averages over 100 m, with the measurements centered at altitudes of 127 m (□), 227 m (○), 320 m (△), 410 m (+), 501 m (◇) and 594 (☆). Two sets of estimated uncertainties in balloon and lidar measurements are shown: these represent the largest and smallest uncertainties computed for these data.

such comparison. This figure shows a common feature of such comparisons: pilot-balloon-derived wind profiles show larger fluctuations than the lidar-derived profiles. Lidar measurements are averaged over 960 m along the lidar beam and over a 5 min time interval. The pilot balloon provides a one point estimate of the wind during the time the balloon rises through the 100 m slab (~30 s). As a result, the lidar gives a better estimate of the mean wind profile than do pilot balloon observations. Fig. 7 presents a comparison of all lidar and pilot balloon measurements made on 19 January 1978. Error estimates shown for the pilot balloon measurements are based on uncertainties in determining pilot balloon positions with the radar. Error estimates for the lidar are the same as for the Madison data. Because all error estimates for data of Fig. 7 are similar, just the largest and the smallest set of error estimates are shown.

The lidar wind measurements show good agreement with simultaneous pilot balloon observations. For all data taken at White Sands on 19 January 1978 the rms errors in speed and direction were 1.1 m $s^{-1}$ and 7°, respectively.

Fig. 8 shows nocturnal wind observations made on 9 January 1978 with both lidar and radar-tracked pilot balloons. These data were obtained on a clear, cold night at White Sands Missile Range. A low-level jet is clearly evident, as is a directional shear of nearly 90° at the top of the layer. Lidar data seg-

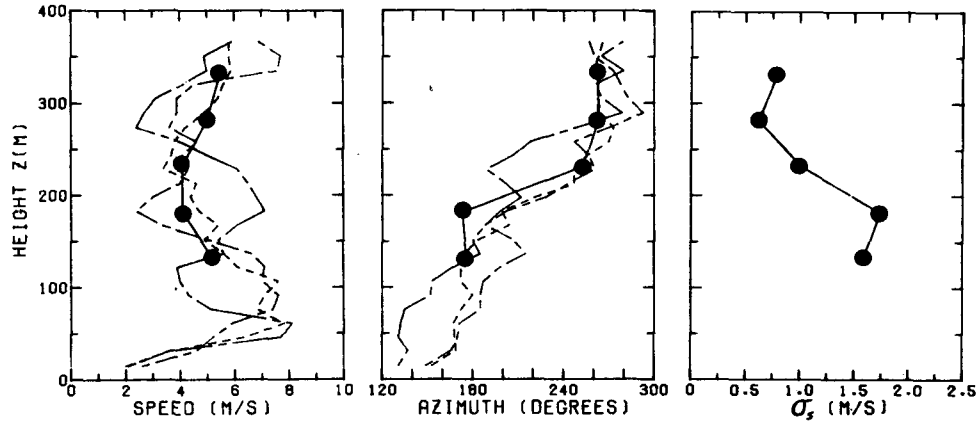


FIG. 8. Wind profiles in the clear nocturnal boundary layer at White Sands, New Mexico on 9 January 1978. Strong directional shear is evident at an altitude of ~200 m. Lidar wind measurements, solid lines (2046–2051 MST) are compared to radar-tracked pilot balloon observations at 2015–2018 MST (-----), 2045–2048 MST (- - - -) and 2105–2108 MST (— - —). Notice that wind shear within the lidar sample volume produces larger values of $\sigma_s$ in this case.

ments of 480 m (32 data points) were used to obtain measurements in 50 m vertical intervals. Above 330 m the signal to noise ratio ($\overline{SNR}$) decreased below 0.5 and lidar wind measurements could not be obtained.

## 4. Conclusion

Experimental results demonstrate the ability of lidar to remotely measure the mean wind speed, direction and rms wind speed fluctuations using naturally occurring aerosol inhomogeneities as tracers. Inhomogeneity scale sizes ranging from 15 to 500 m were found to contain useful wind information. Lidar wind measurements were possible for $\overline{SNR}$ values $> 0.5$. Signal-to-noise ratios are usually adequate to make wind measurements in the clear convective boundary layer at Madison, Wisconsin. Improvement in instrumentation to increase the $\overline{SNR}$ values will increase the range of conditions under which measurements can be obtained.

The fast Fourier transform technique employed for this paper provides wind measurements with a factor of 10 less computer time than the procedure described by Kunkel *et al.* (1980).

*Acknowledgments.* We would like to express our appreciation to the Atmospheric Science Laboratory at the White Sands Missile Range for their cooperation during the experiments conducted there. This research was supported by U.S. Army Research Office Grant DAA-C29-76-C-0156.

## REFERENCES

Armstrong, R. L., J. B. Mason and T. Barber, 1976: Detection of atmospheric aerosol flow using a transit time lidar velocimeter. *Appl. Opt.*, **15**, 2891–2895.

Bingham, C., M. D. Godfrey and J. W. Tukey, 1967: Modern techniques of power spectrum estimation. *IEEE Trans. Audio Electroacoust.*, **15**, 56–66.

Briggs, B. H., G. J. Phillips and D. H. Shin, 1950: The analysis of observations on spaced receivers of fading radio signals. *Proc. Phys. Soc.*, **62**, 106–121.

Comte-Bellot, Genevieve and Stanley Corsin, 1971: Simple Eulerian time correlation of full- and narrow-band velocity signals in grid-generated "isotropic" turbulence. *J. Fluid Mech.*, **48**, 273–337.

Csanady, C. T., 1973: *Turbulent Diffusion in the Environment.* D. Reidel, 248 pp.

Derr, V. E., and C. G. Little, 1970: A comparison of remote sensing of the clear atmosphere by optical, radio, and acoustic radar techniques. *Appl. Opt.*, **9**, 1982–1983.

Eloranta, E. W., J. M. King and J. A. Weinman, 1975: The determination of wind speeds in the boundary layer by monostatic lidar. *J. Appl. Meteor.*, **14**, 1485–1489.

Kunkel, K. E., E. W. Eloranta and J. A. Weinman, 1980: Remote determination of boundary-layer characteristics from lidar measurements. *J. Atmos. Sci.*, **37**, 974–981.

Otness, R. K., and L. D. Enochson, 1972: *Digital Times Series Analysis.* Wiley, 476 pp.

Sroga, J. T., 1979: Remote measurements of boundary-layer velocity parameters by monostatic lidar. ERADCOM Rep. ASL-CR-79-013G-1, Atmos. Sci. Lab., White Sands Missile Range, NM 88002.

Wainstein, L. A., and V. P. Zubakov, 1962: *Extraction of Signals from Noise.* Dover, 382 pp.

Welsh, P. D., 1967: The use of fast Fourier transforms for estimation of power spectra: A method based on time averaging over short, modified periodograms. *Trans. IEEE*, **15**, 70–73.